Magnetic diffuse scattering from Nd above T_N and deduced exchange interaction parameters

2007 J. Phys.: Condens. Matter 19 286201

(http://iopscience.iop.org/0953-8984/19/28/286201)

IOP PUBLISHING JOURNAL OF PHYSICS: CONDENSED MATTER

J. Phys.: Condens. Matter **19** (2007) 286201 (10pp) doi:10.1088/0953-8984/19/28/286201

Magnetic diffuse scattering from Nd above T_N and deduced exchange interaction parameters

Per-Anker Lindgård[1], **Tapan Chatterji**[2], **Karel Prokes**[3], **Vadim Sikolenko**[3] **and Jens-Uwe Hoffmann**[3]

[1] Risø National Laboratory, DK-4000, Roskilde, Denmark
[2] Institut Laue-Langevin, BP 156, 38042 Grenoble Cedex 9, France
[3] Hahn-Meitner Institut, Glienickerstrasse 100, D-14109 Berlin, Germany

Received 11 December 2006, in final form 17 May 2007
Published 26 June 2007
Online at stacks.iop.org/JPhysCM/19/286201

Abstract

The magnetic scattering from a Nd single crystal has been investigated in the temperature range 19–30 K. The maximum at $\boldsymbol{Q} = (-\delta, 1, 0)$ moves continuously from $\delta = 0.145$ at $T_N = 19.9$ K to $\delta = 0.167$ at 25 K. No intensity is found at the $(1 \pm \delta, 0, 0)$ positions. We have deduced the exchange interaction constants, and tested these by successfully calculating the spin wave spectrum. The interaction surface $J(\boldsymbol{q})$ in $\boldsymbol{q}$-space is volcano-like with a sharp, corrugated rim. The structure above 19.1 K, also in the short range ordered phase, is sinusoidal (striped) with no sign of transverse fluctuations. An interesting possibility is that this is a quantum effect. Understanding the nature of this phase may have relevance for understanding the stripe phase in high temperature superconductors.

1. Introduction

The static and dynamic magnetic properties of light rare-earth metal Nd shed new light on the nature of a magnetic sinusoidal phase, also called a stripe phase. It is relevant for understanding the magnetic properties in the high temperature superconducting (HTc) oxides [1–3] (YBCO, LSCO etc), which have been proposed to possess such a state, but the nature thereof is not clear. The magnetism is similar for Nd and the oxides because the strong interactions leave a degenerate, frustrated structure. Hence also the weaker forces are needed to understand the resulting behaviour. That means both the large and very small energy scale must be considered—and be right. The analogy brings a full understanding of the magnetism in Nd to the forefront of present day science. Since the total angular moment is $J = 9/2$ the neutron scattering has two orders of magnitude higher intensity than in the HTc materials and therefore much more information is available. Unfortunately, the understanding of the magnetic properties of Nd has been an unsolved puzzle for almost 50 years. Neutron diffraction

investigations of the magnetic structure of Nd starting by Moon, Cable and Koehler [4] and others [5–9] are numerous. In addition there has been a recent x-ray investigation [10]. These revealed that Nd has the most complicated magnetic structure known for any pure element—including a sinusoidal ordering. The reason for the found complexity has previously not been understood, basically because the magnetic interactions were not determined. This is done here, thereby resolving a large number of the puzzles found in Nd, which show bearings on the puzzles of the HTc materials.

Nd has a double hexagonal close packed crystal structure with the stacking ABAC. In this structure atoms on the A layer have neighbour distribution typical of the cubic structures, whereas those on B and C layers have hexagonal neighbour environments. Nd orders [8] antiferromagnetically at $T_N = 19.9$ K, in a longitudinal sine wave, amplitude modulated phase (LAMP) (similar to the stripe phase [2] proposed for HTc) on the hexagonal sites. However, this is energetically unfavourable for Heisenberg-like exchange interactions, which would rather favour a (flat) spiral phase [11]. In the accompanying paper [12] it is shown that Nd at 10 K indeed has a flat spiral structure on the hexagonal sites, and a weak flat spiral polarization of the cubic sites. For both Nd and the HTc oxides it is hard to find a strong anisotropy, which would appear needed to stabilize a LAMP structure. For Nd the orbital contribution to the isotropic Rudermann–Kittel interaction does according to Kaplan and Lyons [13] give rise to anisotropic two-ion interactions with a strength of about 10% of the isotropic part. These interactions can be expanded in multipoles, and the first and largest term has the symmetry of the classical dipole interaction. The presence of such a term should give an effective sixfold anisotropy even above T_N. However, no experimental evidence for this has been reported. This may be because of a cancellation effect with the classical dipole interaction, which is of similar magnitude. In any case the available data are not sufficient for determining such additional interactions.

The modulation vector for the magnetic ordering is for even ℓ : $\boldsymbol{Q} = (10\ell) - \boldsymbol{\delta}$, where $\boldsymbol{\delta} = \pm\delta(010)$ or $\boldsymbol{\delta} = \pm\delta(-1-10)$. It lies in the basal plane b-direction in real space, and is incommensurate with the crystal structure; at odd ℓ the magnetic ordering is $\boldsymbol{Q} = (00\ell) - \boldsymbol{\delta}$, including also $\boldsymbol{\delta} = \pm\delta(100)$; throughout we use reciprocal lattice units (r.l.u.) and hexagonal indexing. The magnitude $\delta(T)$ decreases monotonically (almost linearly) from $\delta \sim 0.145$ to $\delta \sim 0.11$ from $T = T_N$ to 0.1 K—with signs of lock-in at $\delta = 1/8$ and $1/7$. The temperature dependence is probably due to magnetically induced gaps in the Fermi surface [14], and/or elastic effects, since it continues also above T_N. The magnetic moments lie in the basal plane. The moments on neighbouring hexagonal planes are ordered antiferromagnetically. At $T = T_2 = 19.1$ K a first-order transition to a double-$\boldsymbol{q}$ structure [15, 10, 12] takes place with the wavevector $\boldsymbol{Q} = (00\ell_{odd}) + \boldsymbol{\delta}_1 + \boldsymbol{\delta}_2$, where $\boldsymbol{\delta}_1$ and $\boldsymbol{\delta}_2$ deviate by a temperature dependent, small angle from the (100) and (010) directions and have an angle between them somewhat less than 120°. At $T = T_3 \sim 9$ K the cubic sites order with $\delta_{cub} \sim 0.18$ and a four-$\boldsymbol{q}$ (or more) structure develops. Clearly, there is a strong coupling between the magnetic, the structural and electronic properties. Traditionally, the exchange interactions in magnetic solids have been determined by measuring the spin wave dispersions at temperatures lower than the ordering temperatures by inelastic neutron scattering. However, the exchange interactions in Nd could not be deduced by this method because no well-defined spin wave signals were found by inelastic scattering [16].

It is a bit surprising that no diffuse magnetic neutron scattering [8] at temperatures above T_N has been undertaken on Nd. Critical magnetic neutron scattering samples the short range ordered spin fluctuations and yields diffuse Lorentzian peaks in q-space. The positions and half-widths directly determine the structure and inverse correlation length of the fluctuations. Here we demonstrate that the diffuse magnetic scattering can be very useful and can give supplementary, important information about the magnetic exchange interactions and the relative

stabilities of competing magnetic phases with small energy differences. We have measured diffuse magnetic neutron scattering intensities from Nd above T_N up to $\sim$1.5 T_N and have from these and other data deduced exchange interaction parameters and the corresponding $\boldsymbol{q}$ dependent interaction surface. An interesting additional finding of the present study is that the diffuse magnetic scattering peak is centred just above T_N at the same propagation vector where the Bragg peak appears below T_N. However, the magnitude of the ordering vector increases continuously above T_N, with a marked increase in slope at $T = T_N$. The kink at T_N indicates a magnetic influence, however, the further increase above T_N requires a different mechanism.

2. Experimental methods

Neutron diffraction experiments were carried out on two diffractometers, E2 and E4, of the Berlin Neutron Scattering Centre (BENSC) of the Hahn-Meitner-Institut, Berlin. The diffractometer E4 is a two-axis diffractometer with a single detector which can be lifted out of the scattering plane if necessary. We have however kept the detector in the scattering plane. No energy analysis was possible on this instrument and the results reported are energy integrated as far as that is possible for a three dimensional magnetic system. The diffractometer E2 in its normal mode of operation is also a two-axis diffractometer equipped with a linear multidetector. The diffractometer operates with the flat-cone geometry and provides the possibility of mapping the reciprocal space layer by layer. There also exists the possibility to analyse energy with the monochromator crystals but this set-up was not used during the present investigation. Here we did integrated measurements as well. We mapped the diffuse intensity in the scattering plane with the multidetector. In both diffractometers unpolarized monochromatic neutrons of wavelength $\lambda = 2.4$ Å were obtained with PG(002) graphite monochromator. A 40′ collimator and a PG graphite filter were used to collimate the monochromatic neutron beam and remove higher order wavelength contamination. A 7 g Nd single crystal of linear dimensions of about 1 cm, grown by the Ames Laboratory, was used for the present investigation. The sample was placed in a He cryostat with its crystallographic [001] or [110] axis parallel to the ω axis of the diffractometer.

3. Results from the neutron scattering experiments

Figures 1(a)–(d) show 2D scans over $1/6$ of the first Brillouin zone in the basal plane for several temperatures between $T = 19.6$ and 25 K. These pictures show raw data without the subtraction of the background arising from the nuclear scattering of the sample and also from the materials of the sample environment. The powder lines come from Al sample holder and Al tail of the cryostat. There exist additional streaks due to the monochromator and the linear multidetector. We have not attempted to put the intensity in the absolute scale. They all show essentially isotropically broadened satellites (insets show a four times magnification) and the complete absence of peaks at $(1 \pm \delta, 0, 0)$. The scan (a) at $T = 0.98T_N$ is in the ordered phase, while (b)–(d) are in the short range ordered phase. Figure 1(e) shows the h-scans we performed at several temperatures below T_N around $\boldsymbol{Q} = (-0.145 \pm h, 1, 0)$, which were fitted with a Gaussian. The full width at half-maximum (FWHM) of these reflections were FWHM $= 0.0056 \pm 0.0001$, which represents the experimental resolution. The reflections developed broad Lorentzian 'wings' as T_N was approached. Figure 1(f) shows similar scans at $T \geqslant T_N$ from Nd in the temperature range 20–25 K with much wider scan range than that used to determine Bragg scans shown in figure 1(e). The data in figure 1(f) have been fitted with a Lorentzian line shape to yield the position δ and FWHM, which have been plotted in figure 2. The errors of the least squares fits become very large at temperatures above 22 K and

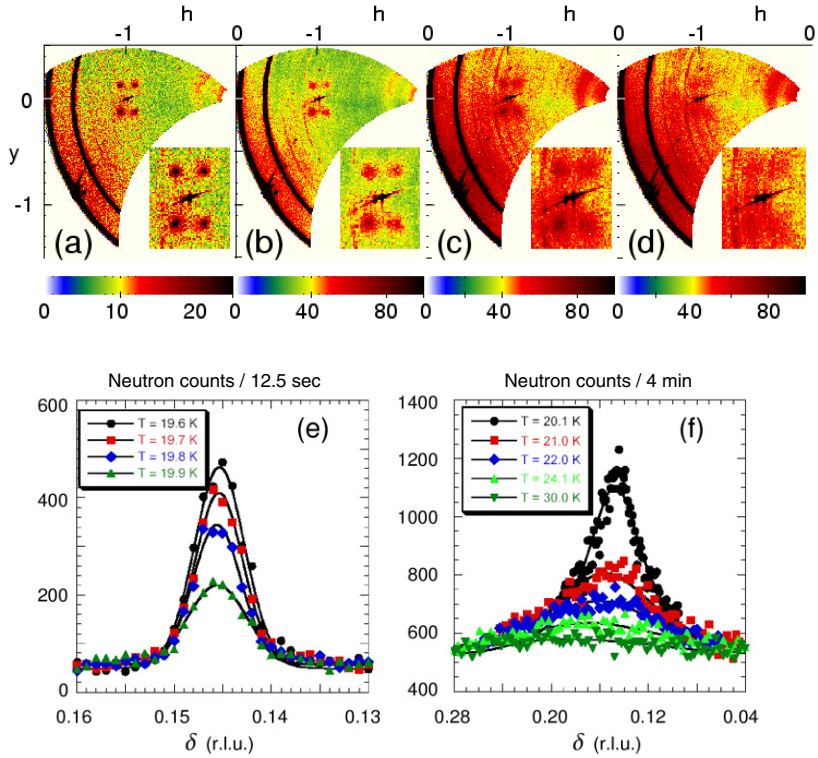

Figure 1. (a)–(d) show 2D scans of the $(h, k, 0)$ plane for ((a), (b), (c), (d)) at $T = (19.6, 20.7, 21.5, 24.1)$ K. The interesting satellite regions are magnified four times in the insets. Notice the total absence of paramagnetic scattering at the $(\pm\delta - 1, 0, 0)$ satellites at all temperatures. It is simply due to the extinction by the $(1 - (\boldsymbol{\kappa} \cdot \mathbf{m})^2)$ factor ($\boldsymbol{\kappa}$ and $\mathbf{m}$ are unit vectors in the scattering- and moment directions). (e) The h-scans of satellite magnetic Bragg reflection of Nd at $\boldsymbol{q} = (-\delta + h, 1, 0)$ at several temperatures below the Néel temperature T_N. The continuous curves are the results of fit of the data with Gaussian curves. (f) h-scans of the magnetic diffuse scattering of Nd at $\boldsymbol{q} = (-\delta + h, 1, 0)$ at several temperatures above the Néel temperature T_N. The continuous curves are the results of fit of the data with Lorentzian curves.

measurements become very difficult and time consuming above about 30 K. Figure 2(a) shows the temperature dependence of the position of diffuse peaks obtained by fitting the data with Lorentzian line shapes. The position of the diffuse scattering maximum at $\boldsymbol{Q} = (-\delta, 1, 0)$ moves continuously from $\delta = 0.145$ at T_N to $\delta = 0.167 \sim 1/6$ at $T = 25$ K. The highest temperature at which we measured the diffuse magnetic intensity from Nd was $T = 30$ K. However, fit of the data with the Lorentzian function does not yield δ and FWHM with any reasonable accuracy.

Figure 2(b) shows the width, FWHM, which is related to the inverse correlation length, κ, by 2κ = FWHM. The instrumental resolution is small, relative to the diffuse scattering above T_N. For example at $T = 21$ K the FWHM is 0.12 ± 0.01, which is about 21 times larger than the instrumental resolution. So, to a very good approximation we can take FWHM given in figure 2(b) as twice the inverse correlation length. The inverse correlation length of Nd at $T = 21$ K is $\kappa = 0.06$, corresponding to a direct correlation length of $\sim$17 lattice units. At $T = 25.2$ K the inverse correlation length $\kappa = 0.14 \pm 0.07$, which gives the direct correlation length of $\sim$7 lattice units. This is about the length of just one magnetic period.

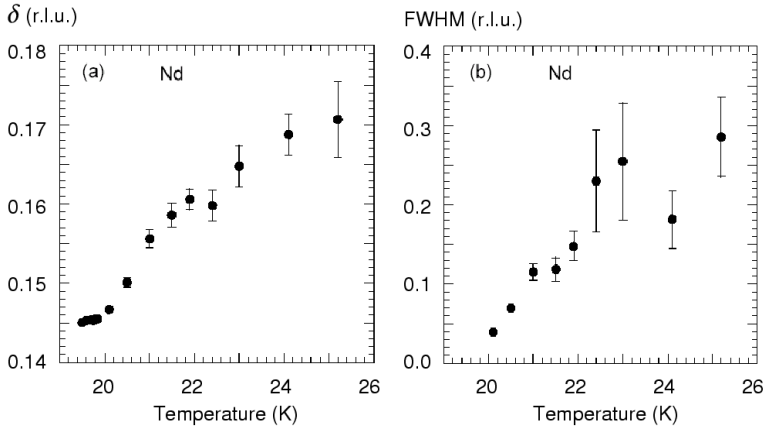

Figure 2. (a) Temperature dependence of the peak position $\boldsymbol{Q} = (-\delta, 1, 0)$ of the magnetic diffuse scattering from Nd obtained by fitting the intensity distribution of figure 1(f) by a Lorentzian function. (b) The full width at the half-maximum (FWHM) of the diffuse magnetic intensity from Nd obtained by fitting the intensity distribution of figure 1(f) by a Lorentzian function.

4. Determination of the exchange interaction parameters

The above data—combined with all information available on the susceptibilities of Nd—can be used to derive information about the exchange interactions in Nd using the mean field (MF) theory. This is possible mainly because of the incommensurate ordering, which on the other hand complicates the spin wave data! Because the information available is very limited, let us assume a minimal Hamiltonian and test how far that brings the analysis:

$$\mathbf{H} = -\sum_{\mathrm{p},\langle ij\rangle} \mathbf{J}^{\mathrm{p}}_{ij} \boldsymbol{J}^{\mathrm{p}}_i \cdot \boldsymbol{J}^{\mathrm{p}}_j + D^{\mathrm{p}} \sum_i J^{\mathrm{p}z2}_i + \mathbf{H}^{\mathrm{h}}_{\mathrm{hex}} + \mathbf{H}_{\mathrm{int}}, \tag{1}$$

where p indicates hexagonal (h) and cubic (c) sites, $D^{\mathrm{h,c}}$ are the axial anisotropy constants and $J^{\mathrm{p}}_{ij} = J^{\mathrm{p}}_n$ are the direct interaction constants in the basal plane between a spin on the hexagonal (or cubic) lattice and its neighbours of group $n = 1, 2, 3, 4, 5$ according to increasing distance. In addition it is possible to determine only one out-of-plane interaction J' between neighbouring hexagonal planes. Therefore, the resulting interactions J_n are effective in-plane interactions, which may include further inter-plane interactions.

The Fourier-transformed interaction function, for $\boldsymbol{q}$ in r.l.u., is for the h sites (x is along the a- and y along the b-direction, i.e. the reciprocal (100) direction):

$$J^{\mathrm{h}}(\boldsymbol{q}) = J(\boldsymbol{q}) + J'(\boldsymbol{q}),$$

where

$$\begin{aligned} J(\boldsymbol{q}) &= 2[J_1(c^x_2 + 2c^x_1 c^y_1) + J_2(c^y_2 + 2c^x_3 c^y_1) + J_3(c^x_4 + 2c^x_2 c^y_2) \\ &\quad + J_5(c^x_6 + 2c^x_3 c^y_3) + 2J_4(c^x_5 c^y_1 + c^x_4 c^y_2 + c^x_1 c^y_3)], \\ J'(\boldsymbol{q}) &= 2J'(e^{y*}_2 + 2c^x_1 e^y_1)\cos(\pi q^z), \end{aligned} \tag{2}$$

where

$$c^x_n = \cos(q^x f n/2), \qquad c^y_n = \cos(q^y f s n/2), \qquad e^y_n = (\mathrm{i}q^y f s n/6),$$
$$f = 4\pi/s,\ s = \sqrt{3}.$$

Because it is not real when including the inter-plane interaction, J', one must use the real value Re {} in equation (3). This fact also complicates the spin wave relations considerably.

Table 1. The deduced exchange constants $J_n^{\rm h}$ between the hexagonal sites n with increasing distance and the inter-planar coupling J'. Using the temperature dependent $\xi = \delta(T) - 0.14$, one may find the interactions corresponding to a temperature where $\delta = \delta(T) \neq 0.14$. Similarly, the deduced coupling between the cubic sites, $J_n^{\rm c}$, is given. For completeness also the axial anisotropy constants are included.

$J_1^{\rm h} = 0.170 \pm 0.02$ K	$+\xi/2$ K	$J_1^{\rm c} = 0.200 \pm 0.02$ K
$J_2^{\rm h} = 0.082 \pm 0.04$ K	$+\xi/2$ K	$J_2^{\rm c} = 0.019 \pm 0.06$ K
$J_3^{\rm h} = 0.062 \pm 0.03$ K	$+\xi/5$ K	$J_3^{\rm c} = 0.023 \pm 0.05$ K
$J_4^{\rm h} = -0.110 \pm 0.02$ K	-2ξ K	$J_4^{\rm c} = -0.071 \pm 0.02$ K
$J_5^{\rm h} = 0.04$ K		$J_5^{\rm c} = 0.04$ K
$J' = -0.080 \pm 0.01$ K	$+\xi$ K	
$D^{\rm h} = 0.77$ K		$D^{\rm c} = 0.12$ K

A similar expression can be written for the interactions on the cubic sites, $J^{\rm c}(\boldsymbol{q})$, which however is real.

We shall later discuss the influence of the small hexagonal and other anisotropy terms $\mathbf{H}_{\rm hex}^{\rm h}$ on the h sites and the weak interaction $\mathbf{H}_{\rm int}$ between the h and c sites, while at first neglecting them. The diffuse magnetic scattering measures the wavevector and temperature dependent susceptibility $\chi(\boldsymbol{q}, T)$ [17, 18]. This can be written in the MF approximation [18]—and the inverse expanded to second order in $\Delta\boldsymbol{q}$ around the maximum at $\boldsymbol{Q}$ as:

$$\chi^{\rm p}(\boldsymbol{q}, T) = {\rm Re}\{1/[C(T - \Delta\Theta^{\rm p}/3) - \mathbf{J}^{\rm p}(\boldsymbol{q})]\} \sim 1/(\boldsymbol{\kappa}^2 + \Delta\boldsymbol{q}^2), \tag{3}$$

where $C = 3k_{\rm B}/S(S+1)$, $k_{\rm B}$ is Boltzmann's constant and $\Delta\Theta^{\rm p} = \Theta_\perp^{\rm p} - \Theta_\parallel^{\rm p}$ are the differences between the Curie–Weiss temperatures for a field in- and out-of-plane for ${\rm p} = {\rm h}, {\rm c}$. They are [19] $\Delta\Theta^{\rm h} = 22.3$ K and $\Delta\Theta^{\rm c} = 3.5$ K. From this we find the anisotropy constants $D^{\rm h} = 0.77$ K, and $D^{\rm c} = 0.12$ K. The Fourier-transformed interaction function $\mathbf{J}^{\rm p}(\boldsymbol{q})$ is complex for the h sites because of the lack of inversion symmetry, but real for the c sites.

The value at $q = 0$ is determined by the Curie–Weiss temperatures as $\mathbf{J}^{\rm p}(0) = C(\Theta_\perp^{\rm p} - \Delta\Theta^{\rm p}/3) = 0.29$ K and 0.85 K for h and c sites, respectively. For example $\mathbf{J}^{\rm h}(0) = 6(J_1^{\rm h}, +J_2^{\rm h} + J_3^{\rm h} + 2J_4^{\rm h} + J_5^{\rm h} + J') = 0.29$ K. Hence, the sum over all interactions is slightly larger than zero for both lattices. Similarly, the Néel temperatures, $T_N^{\rm p}$, determine the maximum of $\mathbf{J}^{\rm p}(\boldsymbol{Q})$, yielding 1.51 K and 0.96 K for h and c sites, respectively. At the peak positions, $\boldsymbol{Q}$, the first derivative of $\mathbf{J}^{\rm p}(\boldsymbol{q})$ is 0 along both the b- and a-direction. This produces several $\boldsymbol{Q}$dependent linear combinations of the parameters to be equal to zero. Finally, the finite values of second derivatives at the peaks are determined by κ from the diffuse scattering, equation (3). From the MF assumption that κ can be written as $\kappa = K(T - T_N^{\rm h})^{1/2}$ we find the amplitude, K from figure 2(b). All conditions are written for the diffuse scattering around $(00\ell_{\rm odd})$ and $(10\ell_{\rm even})$ allowing also J' to be determined. Together with weak conditions that $\mathbf{J}^{\rm p}(\boldsymbol{q})$ must be close to zero in the middle of the zone (to avoid false maxima) we have all together 17 and 11 linear combinations for the h and c sites, respectively, from which we determine $5J_n^{\rm h}$ constants plus J' by using a least squares fit. For the cubic sites we can determine $5J_n^{\rm c}$ interaction parameters—with somewhat less certainty, since less information is available.

Solving the above for the h sites around $\delta = 0.14 + \xi$, where ξ is a small number, yields the exchange constants $J_n^{\rm h}$ between the hexagonal sites n of increasing distance, and the inter-planar J' constant, given in table 1. By finding the experimentally observed ordering vector, yielding $\delta(T) = 0.14 + \xi$ at various temperatures, one can then deduce an estimate also for the temperature dependence of the interaction parameters. The resulting $\mathbf{J}^{\rm h}(\boldsymbol{q})$ function in the

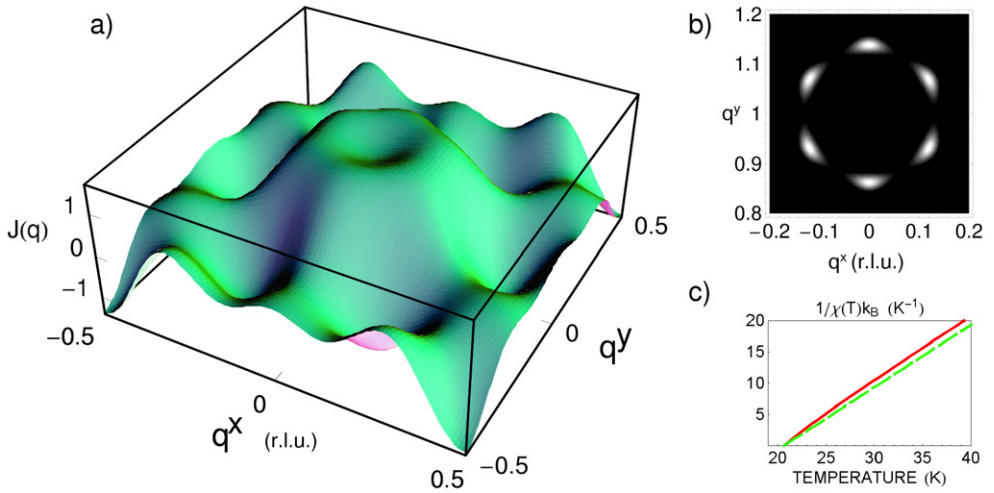

Figure 3. (a) The deduced volcano-like, $\mathbf{J}^{\mathrm{h}}(\boldsymbol{q})$ in K, for the hexagonal sites at $(00\ell_{\mathrm{odd}})$; similar, but 0.7 K lower volcanoes are found at the $(10\ell_{\mathrm{odd}})$ positions; whereas identical ones are found at $(10\ell_{\mathrm{even}})$ and the lower ones at $(00\ell_{\mathrm{even}})$. A similar volcano-like function, $\mathbf{J}^{\mathrm{c}}(\boldsymbol{q})$, is found for the cubic systems with a slightly larger rim radius. (b) The calculated 2D intensity map of $\chi^{\mathrm{h}}(\boldsymbol{Q})$ at $T = 1.01T_{\mathrm{N}}$ around $\boldsymbol{Q} = (1, 0, 0)$. Notice all six satellites are potentially present. (c) The calculated temperature dependences of $1/\chi^{\mathrm{h}}(\boldsymbol{Q}, T)$ at $\boldsymbol{Q} = (\delta, 0, 1)$ and $\boldsymbol{Q} = (\delta, 1, 0)$. Notice the different slopes, which are due to complex interactions between the planes, see equation (2).

$(q^x, q^y, 0)$ plane is shown in figure 3(a). It shows a volcano-like function, with a rim with radius δ and relatively small peaks at all the (100)* directions. The peaks are emphasized by a finite J_5. Introduction of this is needed to provide an almost isotropic intensity pattern, $\chi(\boldsymbol{q})$, around the satellites, See figure 3(b). Hence, we fix $J_5 = 0.04$ K in the fit. If J_5 is reduced to -0.02 K the rim becomes completely flat. Figure 3(c) shows the temperature dependence of inverse susceptibility $1/\chi^{\mathrm{h}}(\boldsymbol{Q}, T)$ at $\boldsymbol{Q} = (\delta, 0, 1)$ and $\boldsymbol{Q} = (1, \delta, 0)$. Notice the different slopes near T_{N}, which are due to complex interactions between the planes. This effect can be used to judge the range of also the inter-planar interactions. A fit for the cubic sites at $\delta^{\mathrm{c}} = 0.18$ yields the effective planar interactions given in table 1. The resulting $\mathbf{J}^{\mathrm{c}}(\boldsymbol{q})$ is again volcano-like with a larger rim radius of 0.18. It is interesting that the cubic nearest neighbour interaction is larger than the hexagonal one. The lower ordering temperature of the cubic sites is due to the smaller planar anisotropy ($D^{\mathrm{c}} < D^{\mathrm{h}}$). Of course the deduced interactions represent only a first approximation to the interactions in Nd. One can therefore not expect these to describe in detail the intricate magnetic phase transitions to multi-q structures observed to occur at lower temperatures. Presumably an important driving force for these is the magnetoelastic interaction and the requirement that the incommensurate magnetic structures must fit in to the dhcp lattice. This will typically involve epitaxial rotation [9, 12], and hence make the ordering vectors deviate from high symmetry directions. It is beyond the present high temperature study to go into such details.

The peak in the $\mathbf{J}^{\mathrm{h,c}}(\boldsymbol{q})$ functions may be more pronounced than here deduced, figure 3. It is due to properties of the Fermi surface, and therefore not easily describable with a few exchange interaction constants. In the neighbouring element, Pr, the interaction function $\mathbf{J}^{\mathrm{h}}(\boldsymbol{q})$ has been measured from the crystal field excitations by neutron scattering [20]. It shows a very pronounced peak. That dispersion relation has been fitted with 22 interaction constants, but still without catching all the details of the minimum of the dispersion relation, which is related to the peak in $\mathbf{J}^{\mathrm{h}}(\boldsymbol{q})$. A similar analysis is of course not possible for Nd with the present available

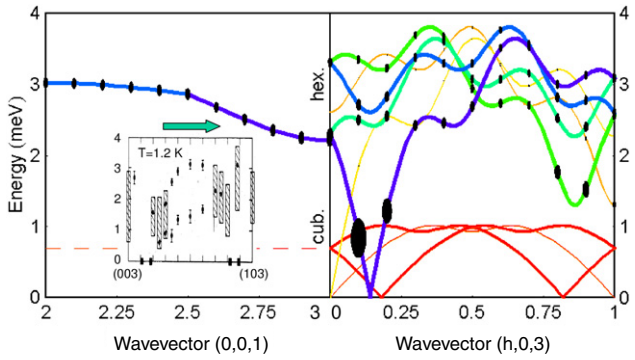

Figure 4. The calculated spin wave dispersion relations for simple spiral structures, based on the deduced exchange interaction parameters and measured planar anisotropies. The hexagonal excitations (bluish and greenish) emerge from the chosen $\delta^{\mathrm{h}} = 0.14$ (actually $\delta \sim 0.11$ is found at $T = 1.2$ K, but the general behaviour—reflecting the volcano-like $\mathbf{J}^{\mathrm{h}}(\boldsymbol{q})$, does not change much with the value of δ). They are split up due to the two sublattices and form a band around 3.5 meV. The calculated relative intensities (without the detailed balance factor) are given by the size of the black ovals. A set of exactly mirrored curves emerging from around (103) are not shown for clarity, but must be added. The thin (yellow) curves emerging from the Bragg peaks carry the intensity factor $(1 - (\boldsymbol{\kappa} \cdot \mathbf{m})^2)$ factor and are therefore very weak close to the ℓ-direction. The cubic modes (reddish) emerge from $\delta^{\mathrm{c}} = 0.18$ and form a band around 1 meV. In most part of the zone there are many nearby branches. At half the zone they cross and leave two narrow signals. Both the scale and the nature of the calculated spectrum are in agreement with experiments [16], shown in the inset.

information. Diffuse scattering has previous been used to determine exchange interactions in simpler systems [21–24], also going beyond the simple mean field theory [23, 24]. Here the analysis is complicated both by the temperature dependent ordering vector, the incommensurate structure and the long ranged interactions. Therefore, we have taken the simplest approach as the first step towards an understanding of the interactions in Nd.

5. Calculated spin wave spectrum at $T = 1.2$ K

It is clear that exchange interaction functions determined from the above information are in general less accurate and unique than those determined from spin wave (or crystal field excitations) measurements in favourable cases. Firstly, because the theory of that is more accurate and secondly because many more $\boldsymbol{q}$-points may be used. However, with the deduced $\mathbf{J}^{\mathrm{h,c}}(\boldsymbol{q})$ functions we can on the other hand, as a test, calculate the spin wave dispersion relations. We have recently deduced [12] that the structure at $T = 10$ K is a 'flat spiral' with an aspect ratio ∼1:3 (and a weak polarization of the cubic sites). The transverse component grows with decreasing temperature. At $T = 1.2$ K we shall therefore assume the magnetic structure to be essentially spiral on both h and c sites, neglecting interactions $\mathbf{H}_{\mathrm{int}}$. For this structure, the dispersion relation is well known [25]. It can been shown numerically that the simplified spiral case discussed there, actually is valid for all, also complex directions of $\boldsymbol{q}$ when using (in their notation) $E_q \pm^2 = |A_q \pm C_q|^2 - |X_q|^2$, where $X_q = B_q \pm D_q$. Hence both energies and intensities can be calculated.

The calculated dispersion relations and intensities are given in figure 4 using the above determined parameters and assuming $\delta^{\mathrm{h}} = 0.14$ and $\delta^{\mathrm{c}} = 0.18$. In agreement with experiments we find two bands of excitations: around 3.5 and 1 meV. Due to the incommensurate order a lot of excitations are found in certain regions of $\boldsymbol{q}$-space (hence difficult to resolve experimentally and in agreement with the observed broad 'bands'), but they cross, and therefore narrow peaks occur at half the zone, precisely as observed by experiments [16] at $T = 1.2$ K, see inset in

figure 4. If the interaction, $\mathbf{H}_{\rm int}$, between the h and c sites is included, the branches interact and gain intensity also in zones, where they are not dominant.

Considering the simplifying assumptions the agreement is surprisingly good. This gives confidence to the parameters and the $\mathbf{J}^{\rm h}(\boldsymbol{q})$, $\mathbf{J}^{\rm c}(\boldsymbol{q})$ functions here obtained by alternative methods. On this basis we can understand the multiple splitting of the peaks in Nd with decreasing temperature below $T = 19.1$ K, since it costs very little energy to move along the rim of the volcanos to accommodate the incommensurate magnetic structure into the lattice. Qualitatively similar $J(\boldsymbol{q})$ volcano-like functions are found in the HTs oxides [3] and this establishes a profound analogy between those and Nd, although the former are yet still more complicated.

6. Absence of transverse paramagnetic scattering in Nd

A very interesting behaviour of Nd is actually found for $T > 19.1$ K, where the present experiments are focused. The present neutron scattering results show total absence of diffuse scattering of intensity along the (100) direction, see figures 1(a)–(d). This is the proof of the sinusoidal LAMP order in Nd. In MF theory this is the natural end of a flat spiral cite12 near $T_{\rm N}$: spins in the transverse, small moment regions experience a relatively small MF and go disordered before the longitudinal regions. Hence, a small two-ion anisotropy, sixfold anisotropy or magnetoelastic coupling, $\mathbf{H}^{\rm h}_{\rm hex}$ (yielding a distorted spiral) can, together with an incommensurate ordering vector, indeed be the driving force, because the effect thereof is strongly enhanced by temperature close to, but below $T_{\rm N}$. However, even at $T = 1.5T_{\rm N}$ no transverse scattering is observed, which would be expected in case of 'ordinary' paramagnetic scattering, where the spins fluctuate in all directions. Hence, we are lead to conclude that the transverse Nd moments seem to 'disappear' in the low moment regions! This should be investigated further—and be quantified. A sixfold or two-ion anisotropy, for example of dipolar symmetry, may have the effect of reducing the transverse fluctuations also in a short range ordered phase. But they cannot totally suppress them. Further, in this case a significant sixfold anisotropy of the susceptibility should be observable above $T_{\rm N}$, which has not been measured. An interesting possibility is quantum effects. That is dominant in the neighbouring element, Pr with $J = 4$. This forms a non-magnetic singlet $|0\rangle$ ground state on each site, and no spontaneous magnetic ordering exist in the pure Pr. On the other hand this allows crystal field excitations to be fully measured. Nd, having a non-integer $J = 9/2$, instead forms a $|\pm 1/2\rangle$ Kramers doublet to minimize the moment in the large axial crystal field. However the moment is not vanishing, therefore a description in terms of a planar anisotropy constant is valid. The next energy level $|\pm 3/2\rangle$ is expected to be only around 0.5 meV above [16]. Inelastic neutron scattering measurements [16] detect considerable amount of low energy scattering, but have failed to detect a clear crystal field transition between the mentioned levels above $T_{\rm N}$. Somewhat similar to Pr, it is possible that Nd may produce 'vanishing' moments at certain pair of sites by forming singlet pairs, and thereby gain exchange energy relative to the paramagnetic state. MF theory cannot distinguish between paramagnetic and singlet disorder. Such singlets will not show any elastic neutron signal. However, there should be inelastic excitations at around $2J'J^2 \sim 0.3$ meV—with a characteristic form factor. This brings the contact to the HTc materials where a similar 'stripe' or LAMP sinusoidal phase has been proposed [2]. In that case the spins are simply $S = 1/2$ and quantum effects, such as singlet pair formations, are naturally to be expected. We emphasize: in Nd the LAMP sinusoidal order is fluctuation dominated, and found only within 4% of $T_{\rm N}$, or as short range order (of range of 17–7 sites) above. Hence, one finds only small domains of this order and not a complete stripe phase. It might be worthwhile to further study the properties of the sinusoidal phase in Nd, also with inelastic scattering, for the range $19\ {\rm K} < T < 30\ {\rm K}$.

7. Conclusions

The present study has resulted in valuable, new information about the exchange interactions in Nd, which is new and interesting in its own right. The analysis allows determination of the presumably dominant isotropic interactions, but cannot resolve possible weaker interactions like two-ion anisotropy and magnetoelastic forces. The found volcano-like interaction surface rationalizes the particular and exceptional magnetic behaviour of Nd, where a multitude of satellites are found at low temperatures. This is possible because the ordering vector may deviate from symmetry directions at low cost of magnetic energy (epitaxial rotation) to minimize elastic energy. However, much wider, understanding the Nd structure gives an insight into other incommensurate magnetic structures, for example those proposed to be important for understanding the HTc materials, which have a similar interaction surface as the one found for Nd. Very surprisingly, there is absolutely no sign of transverse scattering even at $T = 1.5T_N$. If the low moment regions were occupied by paramagnetic ions one would expect a measurable intensity at $T > T_N$. This might indicate that the Nd ions prefer to form non-magnetic singlet pairs, which cannot be observed by elastic neutron scattering. This is close to the singlet state proposed by Anderson [26] for the HTc materials. Further studies of Nd could clarify the nature of such a state with the advantage of much larger intensities.

Acknowledgments

This research has been supported by the European Commission under the Access to Research Infrastructures Action of the Human Potential Programme (Contract no. HPRI-CT-2001-00138).

References

[1] Hayden S M, Mook H A, Dai V, Perring T G and Dogan F 2004 *Nature* **429** 531
[2] Tranquada J M *et al* 2004 *Nature* **429** 534
[3] Lindgård P-A 2005 *Phys. Rev. Lett.* **95** 217001
[4] Moon R M, Cable J W and Koehler W C 1964 *J. Appl. Phys.* **35** 1041
[5] Bak P and Lebech B 1978 *Phys. Rev. Lett.* **40** 800
[6] Moon R M, Koehler W C, Sinha S K, Stassis C and Kline G R 1979 *Phys. Rev. Lett.* **43** 62
[7] Lebech B and Als-Nielsen J 1980 *J. Magn. Magn. Mater.* **469/470** 15
[8] Lebech B 1981 *J. Appl. Phys.* **52** 2019
[9] Lebech B, Woolny J and Moon R M 1994 *J. Phys.: Condens. Matter* **6** 5201
[10] Watson D, Nuttall W J, Forgan E M, Perry S C and Fort D 1998 *Phys. Rev.* B **57** R8095
[11] Lindgård P-A 1997 *Phys. Rev. Lett.* **78** 4641
[12] Lindgård P-A 2007 *J. Phys.: Condens. Matter* **19** 286202
[13] Kaplan T A and Lyons D H 1963 *Phys. Rev.* **129** 2072
[14] Elliott R J and Wedgwood F A 1964 *Proc. Phys. Soc.* **84** 63
[15] McEwen K A, Forgan E M, Stanley H B, Bouillot J and Fort D 1985 *Physica* B **130** 362
[16] McEwen K A and Stirling W G 1982 *J. Magn. Magn. Mater.* **30** 99
Stirling W G, McEwen K A and Stanley H B 1985 *J. Appl. Phys.* **57** 3756
[17] Lindgård P-A 1978 *Neutron Diffraction* ed H Dachs (Berlin: Springer) pp 197–242
[18] Collins M F (ed) 1989 *Magnetic Critical Scattering* (Oxford: Oxford University Press)
[19] Stanley H B, Brown P J, McEwen K A and Rainford B D 1986 *Physica* B **136** 400
[20] Houmann J G, Rainford R D, Jensen J and Mackintosh A R 1979 *Phys. Rev.* B **20** 1105
[21] Chattopaddhyay T, Brückel T and Burlet P 1993 *Phys. Rev.* B **44** 7394
[22] Chatterjee T, Schneider R, Hoffmann J-U, Hohlwein D, Suryanarayanan R, Dhalenn G and Revcolevschi A 2002 *Phys. Rev.* B **65** 134440
[23] Hohlwein D, Hoffmann J-U and Schneider R 2003 *Phys. Rev.* B **68** 140408
[24] Hohlwein D 2002 *Appl. Phys.* A **74** 740
[25] Lindgård P-A, Kowalska A and Laut P 1967 *J. Phys. Chem. Solids* **28** 1357
[26] Anderson P W, Lee P A, Randeria M, Rice T M, Trivedi N and Zhang F Z 2004 *J. Phys.: Condens. Matter* **16** R755